Flow Boiling Heat Transfer Characteristics of R134a in a Horizontal Mini Tube[†]

Lihong Wang,[‡] Min Chen,*[,‡] and Manfred Groll[§]

Department of Engineering Mechanics, Tsinghua University, Beijing 100084, China, and Institute of Nuclear Energy & Energy Systems, University of Stuttgart, Stuttgart 70569, Germany

Flow boiling heat transfer characteristics of 1,1,1,2-tetrafluoroethane (R134a) were experimentally investigated in a horizontal stainless steel mini tube. The inner diameter of the test tube is 1.3 mm, and the tube wall thickness is 0.1 mm. Local heat transfer coefficients are obtained over a range of vapor qualities up to 0.8, mass fluxes from (310 to 860) $kg \cdot m^{-2} \cdot s^{-1}$, heat fluxes from (21 to 50) $kW \cdot m^{-2}$, and saturation pressures from (0.65 to 0.75) MPa. The dependences of heat transfer coefficients on mass flux, heat flux, saturation pressure, and vapor quality are demonstrated. On the basis of an available model in recent literature, potential heat transfer mechanisms are also analyzed.

1. Introduction

Over the past decades, compact heat exchangers, because of their remarkable advantages such as higher heat transfer area density, small size, and better heat transfer characteristics, are gaining increasing attention.[1−3] Extensive applications exist in industries where more compact heat exchangers with a two-phase operation may provide higher performance and better flexibility to remove heat than those employing a single-phase operation, such as the potential applications in thermal control of spacecraft payloads and other aerospace areas.[4] Meanwhile, microscale heat exchangers are becoming necessary in many microelectronic mechanical systems (MEMS), which are very sensitive to temperature.

In recent years, a number of researchers have carried out experiments on flow boiling heat transfer in mini-size tubes and channels. An experiment on flow boiling heat transfer of refrigerant 1,1,2-trichlorotrifluoroethane (R113) in a horizontal tube with an inner diameter of 2.92 mm was conducted by Wambsganss et al.[5] They reported that, for saturated boiling, the heat transfer coefficient was strongly dependent on the heat flux and hardly dependent on the vapor quality. Oh et al.[6] studied the saturated flow boiling heat transfer for 1,1,1,2-tetrafluoroethane (R134a) in horizontal tubes with inner diameters of 0.75 mm, 1 mm, and 2 mm. They observed that the heat transfer coefficient was a strong function of vapor quality. In the low quality region, the measured heat transfer coefficient increased rather slowly with quality, whereas in the higher quality region there was a relatively rapid increase in the heat transfer coefficient when quality increased. The local flow boiling heat transfer of 1,1-dichloro-1-fluoroethane (R141b) was investigated in horizontal tubes with diameters of (1.39 to 3.69) mm by Kew and Cornwell.[3] Their experiments demonstrated that the heat transfer coefficient had a strong dependence upon vapor quality in the higher quality region and there was negligible influence of vapor quality in the lower quality region. The independently measured heat transfer coefficients by Zhang et al.[7] and Bertsch et al.[8] also drew the same conclusion. An experiment on flow boiling was conducted by Lin et al.,[9] with R141b in a tube with diameter of 1 mm. They found that under low heat flux the heat transfer coefficient was almost constant with increasing quality while under high heat flux the heat transfer coefficient sharply decreased with increasing quality in the whole saturated boiling region. Huo et al.[10] performed a flow boiling experiment in a small tube with R134a and obtained a similar result as that of Lin et al.[9] Recently, Shiferaw et al.[11] carried out flow boiling experiments and compared their results with a three-zone evaporation model developed by Thome et al. The comparison indicated that the flow boiling heat transfer coefficient decreased with the vapor quality increase, especially at low pressures.

It is noticeable that the boiling heat transfer characteristics obtained so far for mini-size channels are in poor agreement or even in contradiction to each other. Our understanding of the physical mechanisms behind those experiments is not sufficient to allow a deep and comprehensive analysis. Consequently, the experiments described in the following are carried out as part of a project aimed to clarify the flow boiling heat transfer mechanisms in small channels. Some contradictions about boiling heat transfer mechanisms in small channels will be reconciled, in part, by the results of this study.

2. Experimental Apparatus and Procedures

The experimental apparatus is schematically shown in Figure 1, which consists of four main systems, namely, the refrigerant loop, the cooling water loop, the direct current (DC) power supply for heating the test section, and a data acquisition system. Refrigerant R134a is circulated in the refrigerant loop. The cooling water loop has enough cooling capacity to remove the heat generated by the DC power supply and regulate the inlet temperature of the test section.

The refrigerant loop contains a reservoir, a magnetic pump, a volume flow meter, a test section, and two condensers. The working fluid is pumped in the refrigerant loop by a magnetic pump with rated output. By adjusting the fine valve and coarse valve simultaneously, the flow rate can be regulated. The excess fluid flows back to the reservoir through the coarse valve while the wanted part flows through the fine valve, fine condenser, flow meter, test section, coarse condenser, and reservoir in sequence, thus completing a circulation. The coarse condenser with larger cooling capacity is used to condense the vapor from

[†] Part of the "William A. Wakeham Festschrift".

* Corresponding author. E-mail: mchen@tsinghua.edu.cn. Tel.: +86 1062773776. Fax: +86 1062795832.
[‡] Tsinghua University.
[§] University of Stuttgart.

10.1021/je900140w CCC: $40.75
Published on Web 07/28/2009

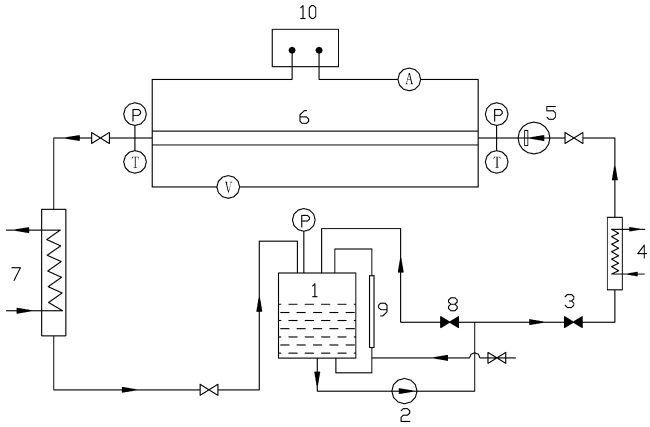

Figure 1. Schematic diagram of the experimental system: 1, reservoir; 2, magnetic pump; 3, fine valve; 4, fine condenser; 5, flow meter, 6, test section; 7, coarse condenser; 8, coarse valve; 9, sight glass; 10, DC power supply.

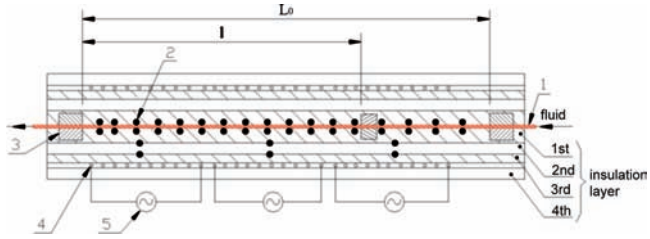

Figure 2. Schematic diagram of the test section: 1, stainless steel tube; 2, thermocouples; 3, copper sleeves of DC power supply; 4, electrical resistance; 5, AC power supply.

the test section. At the same time, the fine condenser controls the inlet temperature of the working fluid. The flow rate is measured by the volume flow meter by McMillan Company with an accuracy of 0.8 % in the range of (13 to 100) mL·min^{-1}. In addition, pressures at inlet and outlet are measured by a pressure difference transducer with an uncertainty of 0.1 %, in the range of (0 to 1.2) MPa.

As schematically shown in Figure 2, the test section is a horizontal stainless steel tube with an inner diameter (D_h) of 1.3 mm and a thickness (δ) of 0.1 mm. The heated length (L_0) of the test section is 720 mm. To reach the high heat flux working condition, a subtest section with a heated length (l) of 480 mm is adopted. DC electrical power is supplied to the stainless steel tube sections via copper sleeves to obtain a uniform heat flux boundary condition. The copper sleeves are silver brazed to the ends of each tube section and have been sized to produce negligible heat generation compared with the heat generated in the stainless tube. The voltage drop across the test section is measured directly across the copper sleeves, whereas the current is determined by putting a calibrated resistance in series with the test section and measuring the voltage across it. Outer wall temperatures of the test section and the subtest section are measured at 17 and 13 axial locations along the length of the tube, respectively, by copper−constantan thermocouples with a calibrated uncertainty of 0.05 °C. At each location, two thermocouples are symmetrically located at the top and the bottom of the tube. All thermocouples are pasted to the outside surface of the tube with electrically insulating glue. Four layers of thermal-insulating material and three segments of thermal guards are wrapped around the outside surface of the test section to reduce the heat loss. Each of the three segments of thermal guards consists of an electrical resistance, an alternating current (AC) power supply, and a temperature-difference feedback system. The three thermal guard segments keep the difference in temperature between the inside and the outside of the second layer of insulating thermal material as small as possible, which insures that the outside surface boundary condition is as close as thermal insulated. All experimental data are collected by a data acquisition system with an uncertainty of ± 0.5 %. The thermophysical properties of the working fluid were taken from the ASHRAE Handbook Fundamentals 2005.[12]

3. Data Reduction

Prior to performing flow boiling heat transfer experiments, single-phase heat transfer experiments are carried out to check the experimental system and to calibrate the heat loss. The results demonstrate that the system is reliable and the heat loss is less than 1.5 %. Considering the small tube wall thickness (0.1 mm), axial heat conduction will not be taken into account. The local heat transfer coefficient, at position z along the length of the tube, is defined as eq 1.

$$h(z) = \frac{q}{T_{wi}(z) - T_{sat}(z)} \tag{1}$$

where h is the heat transfer coefficient and the inner wall temperature of the tube $T_{wi}(z)$ is obtained from eq 2 by taking the tube outside surface as insulated.

$$T_{wi}(z) = \frac{1}{2}\frac{q}{k_s} r \left[-\frac{\left(\frac{r}{r_0}\right)^2 - 2\ln\left(\frac{r}{r_0}\right) - 1}{1 - \left(\frac{r}{r_0}\right)^2} \right] + T_{wo}(z) \tag{2}$$

In eq 1, linear interpolation is applied to determine the fluid saturation pressures at each measurement location along the test tube, after which the fluid saturation temperatures $T_{sat}(z)$ are determined. Tran et al.[13] verified that an error was hardly introduced using the linear pressure drop.

The length of the subcooled inlet region is calculated iteratively

$$L_{osb} = \frac{GD_h C_p (T_{sat}^{osb} - T_{in})}{4q} \tag{3}$$

where C_p is the specific heat capacity at constant pressure, D_h the tube hydraulic diameter, G the mass flux, and q the heat flux. The local vapor quality at positions $x(z)$ is determined by a thermal balance from the equation

$$x(z) = \frac{q\pi D_h (z - L_{osb})}{h_{fg} AG} \tag{4}$$

where A is the tube flow area, L the length of the test section, and h_{fg} the specific enthalpy of vaporization.

The process of uncertainty analysis described by Moffat[14] is used to estimate the experimental uncertainties in this study. On the basis of the calibrations of the entire temperature measurements, including thermocouples and the data acquisition system, the uncertainties associated with the temperature and temperature difference data are ± 0.19 °C and ± 0.27 °C, respectively. The uncertainty in heat flux, which depends on the measurements of the voltage and the current across the test section, is 0.24 %. The uncertainty in the refrigerant mass flux is 1.8 %. Consequently, the experimental uncertainty in the heat transfer coefficient is estimated to be under ± 12.0 % for low heat flux measurements and about ± 10.3 % for a moderate mass and heat flux run.

Table 1. Measured Local Heat Transfer Coefficient h under Average Saturation Pressure p, Heat Flux q, Mass Flux G, and Vapor Quality x

no.	p / MPa	q / kW·m^{-2}	G / kg·m^{-2}·s^{-1}	x	h / kW·m^{-2}·K^{-1}	no.	p / MPa	q / kW·m^{-2}	G / kg·m^{-2}·s^{-1}	x	h / kW·m^{-2}·K^{-1}
1	0.651	50.0	836	0.031	14.638	184	0.675	30.0	400	0.685	8.330
2	0.651	50.0	836	0.073	14.261	185	0.675	30.0	400	0.737	8.294
3	0.651	50.0	836	0.114	13.988	186	0.675	30.0	400	0.789	7.347
4	0.651	50.0	836	0.155	13.515	187	0.675	30.0	400	0.816	6.210
5	0.651	50.0	836	0.197	13.146	188	0.675	25.4	518	0.012	7.370
6	0.651	50.0	836	0.238	12.480	189	0.675	25.4	518	0.054	7.200
7	0.651	50.0	836	0.280	12.217	190	0.675	25.4	518	0.097	7.160
8	0.651	50.0	836	0.321	12.074	191	0.675	25.4	518	0.130	7.240
9	0.651	50.0	836	0.363	11.951	192	0.675	25.4	518	0.164	7.310
10	0.651	50.0	836	0.384	11.869	193	0.675	25.4	518	0.198	7.280
11	0.675	50.0	676	0.008	14.401	194	0.675	25.4	518	0.232	7.360
12	0.675	50.0	676	0.059	13.972	195	0.675	25.4	518	0.266	7.390
13	0.675	50.0	676	0.110	13.553	196	0.675	25.4	518	0.300	7.430
14	0.675	50.0	676	0.162	13.185	197	0.675	25.4	518	0.334	7.380
15	0.675	50.0	676	0.213	12.475	198	0.675	25.4	518	0.368	7.440
16	0.675	50.0	676	0.264	12.379	199	0.675	25.4	518	0.401	7.410
17	0.675	50.0	676	0.315	12.293	200	0.675	25.4	518	0.435	7.480
18	0.675	50.0	676	0.367	12.278	201	0.675	25.4	518	0.469	7.470
19	0.675	50.0	676	0.418	12.192	202	0.675	25.4	518	0.487	7.510
20	0.675	50.0	676	0.469	12.087	203	0.675	25.4	370	0.011	7.574
21	0.675	50.0	676	0.496	11.980	204	0.675	25.4	370	0.070	7.519
22	0.675	50.0	621	0.013	14.816	205	0.675	25.4	370	0.129	7.290
23	0.675	50.0	621	0.068	14.298	206	0.675	25.4	370	0.189	7.306
24	0.675	50.0	621	0.124	13.856	207	0.675	25.4	370	0.236	7.355
25	0.675	50.0	621	0.180	13.426	208	0.675	25.4	370	0.284	7.384
26	0.675	50.0	621	0.236	12.693	209	0.675	25.4	370	0.331	7.383
27	0.675	50.0	621	0.292	12.513	210	0.675	25.4	370	0.379	7.452
28	0.675	50.0	621	0.348	12.416	211	0.675	25.4	370	0.426	7.470
29	0.675	50.0	621	0.404	12.329	212	0.675	25.4	370	0.474	7.387
30	0.675	50.0	621	0.460	12.232	213	0.675	25.4	370	0.521	7.486
31	0.675	50.0	621	0.516	12.064	214	0.675	25.4	370	0.569	7.484
32	0.675	50.0	621	0.545	11.960	215	0.675	25.4	370	0.616	7.511
33	0.675	50.0	836	0.023	14.901	216	0.675	25.4	370	0.664	7.449
34	0.675	50.0	836	0.064	14.521	217	0.675	25.4	370	0.711	7.527
35	0.675	50.0	836	0.106	14.247	218	0.675	25.4	370	0.736	7.530
36	0.675	50.0	836	0.147	13.768	219	0.675	25.0	676	0.014	7.380
37	0.675	50.0	836	0.189	13.396	220	0.675	25.0	676	0.047	7.360
38	0.675	50.0	836	0.230	12.721	221	0.675	25.0	676	0.073	7.330
39	0.675	50.0	836	0.272	12.456	222	0.675	25.0	676	0.098	7.320
40	0.675	50.0	836	0.313	12.314	223	0.675	25.0	676	0.124	7.350
41	0.675	50.0	836	0.355	12.192	224	0.675	25.0	676	0.150	7.400
42	0.675	50.0	836	0.376	12.110	225	0.675	25.0	676	0.176	7.390
43	0.675	50.0	463	0.071	14.645	226	0.675	25.0	676	0.202	7.410
44	0.675	50.0	463	0.146	13.865	227	0.675	25.0	676	0.228	7.450
45	0.675	50.0	463	0.221	13.099	228	0.675	25.0	676	0.254	7.420
46	0.675	50.0	463	0.296	12.664	229	0.675	25.0	676	0.280	7.480
47	0.675	50.0	463	0.371	12.413	230	0.675	25.0	676	0.306	7.470
48	0.675	50.0	463	0.446	12.265	231	0.675	25.0	676	0.332	7.490
49	0.675	50.0	463	0.521	12.067	232	0.675	25.0	676	0.345	7.530
50	0.675	50.0	463	0.596	11.920	233	0.675	25.0	527	0.012	7.370
51	0.675	50.0	463	0.671	11.794	234	0.675	25.0	527	0.053	7.200
52	0.675	50.0	463	0.746	11.639	235	0.675	25.0	527	0.095	7.160
53	0.675	50.0	463	0.786	9.860	236	0.675	25.0	527	0.128	7.240
54	0.675	50.0	518	0.041	14.360	237	0.675	25.0	527	0.162	7.310
55	0.675	50.0	518	0.109	13.480	238	0.675	25.0	527	0.195	7.280
56	0.675	50.0	518	0.177	12.920	239	0.675	25.0	527	0.228	7.360
57	0.675	50.0	518	0.244	12.640	240	0.675	25.0	527	0.262	7.390
58	0.675	50.0	518	0.312	12.340	241	0.675	25.0	527	0.295	7.430
59	0.675	50.0	518	0.380	12.190	242	0.675	25.0	527	0.328	7.380
60	0.675	50.0	518	0.448	12.080	243	0.675	25.0	527	0.362	7.440
61	0.675	50.0	518	0.516	11.990	244	0.675	25.0	527	0.395	7.410
62	0.675	50.0	518	0.584	11.889	245	0.675	25.0	527	0.428	7.480
63	0.675	50.0	518	0.652	11.780	246	0.675	25.0	527	0.462	7.470
64	0.675	50.0	518	0.687	11.700	247	0.675	25.0	527	0.479	7.510
65	0.675	42.9	518	0.022	12.230	248	0.675	21.1	518	0.026	6.500
66	0.675	42.9	518	0.079	11.730	249	0.675	21.1	518	0.071	6.470
67	0.675	42.9	518	0.136	11.640	250	0.675	21.1	518	0.096	6.490
68	0.675	42.9	518	0.194	11.550	251	0.675	21.1	518	0.125	6.510
69	0.675	42.9	518	0.251	11.470	252	0.675	21.1	518	0.153	6.410
70	0.675	42.9	518	0.309	11.390	253	0.675	21.1	518	0.181	6.580
71	0.675	42.9	518	0.366	11.330	254	0.675	21.1	518	0.210	6.670
72	0.675	42.9	518	0.423	11.270	255	0.675	21.1	518	0.238	6.530
73	0.675	42.9	518	0.481	11.240	256	0.675	21.1	518	0.267	6.780

Table 1. Continued

no.	p / MPa	q / kW·m^{-2}	G / kg·m^{-2}·s^{-1}	x	h / kW·m^{-2}·K^{-1}	no.	p / MPa	q / kW·m^{-2}	G / kg·m^{-2}·s^{-1}	x	h / kW·m^{-2}·K^{-1}
74	0.675	42.9	518	0.538	11.180	257	0.675	21.1	518	0.295	6.720
75	0.675	42.9	518	0.568	11.130	258	0.675	21.1	518	0.323	6.850
76	0.675	35.1	518	0.001	10.500	259	0.675	21.1	518	0.352	6.870
77	0.675	35.1	518	0.048	10.370	260	0.675	21.1	518	0.380	7.030
78	0.675	35.1	518	0.095	10.250	261	0.675	21.1	518	0.395	7.060
79	0.675	35.1	518	0.142	10.160	262	0.696	50.0	836	0.017	15.122
80	0.675	35.1	518	0.189	10.110	263	0.696	50.0	836	0.058	14.739
81	0.675	35.1	518	0.236	10.070	264	0.696	50.0	836	0.100	14.463
82	0.675	35.1	518	0.282	10.020	265	0.696	50.0	836	0.142	13.980
83	0.675	35.1	518	0.329	9.970	266	0.696	50.0	836	0.184	13.604
84	0.675	35.1	518	0.376	9.920	267	0.696	50.0	836	0.226	12.921
85	0.675	35.1	518	0.423	9.870	268	0.696	50.0	836	0.267	12.654
86	0.675	35.1	518	0.448	9.840	269	0.696	50.0	836	0.309	12.512
87	0.675	35.1	676	0.012	10.179	270	0.696	50.0	836	0.351	12.391
88	0.675	35.1	676	0.048	10.135	271	0.696	50.0	836	0.373	12.308
89	0.675	35.1	676	0.084	10.111	272	0.696	50.0	463	0.061	14.935
90	0.675	35.1	676	0.120	9.988	273	0.696	50.0	463	0.137	14.142
91	0.675	35.1	676	0.156	10.012	274	0.696	50.0	463	0.213	13.363
92	0.675	35.1	676	0.192	10.007	275	0.696	50.0	463	0.289	12.920
93	0.675	35.1	676	0.228	10.012	276	0.696	50.0	463	0.365	12.667
94	0.675	35.1	676	0.264	10.007	277	0.696	50.0	463	0.441	12.518
95	0.675	35.1	676	0.300	9.992	278	0.696	50.0	463	0.518	12.318
96	0.675	35.1	676	0.319	9.970	279	0.696	50.0	463	0.594	12.170
97	0.675	35.1	436	0.031	10.473	280	0.696	50.0	463	0.670	12.043
98	0.675	35.1	436	0.087	10.330	281	0.696	50.0	463	0.746	11.886
99	0.675	35.1	436	0.142	10.188	282	0.696	50.0	463	0.786	10.071
100	0.675	35.1	436	0.198	10.125	283	0.701	30.0	400	0.009	8.734
101	0.675	35.1	436	0.254	10.063	284	0.701	30.0	400	0.074	8.663
102	0.675	35.1	436	0.310	9.991	285	0.701	30.0	400	0.139	8.634
103	0.675	35.1	436	0.366	9.928	286	0.701	30.0	400	0.204	8.636
104	0.675	35.1	436	0.422	9.876	287	0.701	30.0	400	0.256	8.558
105	0.675	35.1	436	0.478	9.824	288	0.701	30.0	400	0.308	8.595
106	0.675	35.1	436	0.534	9.761	289	0.701	30.0	400	0.360	8.549
107	0.675	35.1	436	0.563	9.710	290	0.701	30.0	400	0.412	8.544
108	0.675	35.1	365	0.057	10.201	291	0.701	30.0	400	0.464	8.467
109	0.675	35.1	365	0.123	10.055	292	0.701	30.0	400	0.516	8.504
110	0.675	35.1	365	0.190	9.949	293	0.701	30.0	400	0.568	8.416
111	0.675	35.1	365	0.257	9.920	294	0.701	30.0	400	0.620	8.473
112	0.675	35.1	365	0.324	9.862	295	0.701	30.0	400	0.672	8.489
113	0.675	35.1	365	0.390	9.824	296	0.701	30.0	400	0.724	8.453
114	0.675	35.1	365	0.457	9.755	297	0.701	30.0	400	0.776	7.488
115	0.675	35.1	365	0.524	9.697	298	0.701	30.0	400	0.803	6.330
116	0.675	35.1	365	0.591	9.648	299	0.705	25.4	370	0.055	7.721
117	0.675	35.1	365	0.657	9.619	300	0.705	25.4	370	0.113	7.664
118	0.675	35.1	365	0.692	9.580	301	0.705	25.4	370	0.172	7.431
119	0.675	35.1	333	0.002	10.504	302	0.705	25.4	370	0.219	7.450
120	0.675	35.1	333	0.075	10.347	303	0.705	25.4	370	0.266	7.500
121	0.675	35.1	333	0.148	10.166	304	0.705	25.4	370	0.312	7.528
122	0.675	35.1	333	0.221	10.096	305	0.705	25.4	370	0.359	7.526
123	0.675	35.1	333	0.294	10.005	306	0.705	25.4	370	0.406	7.596
124	0.675	35.1	333	0.367	9.924	307	0.705	25.4	370	0.453	7.614
125	0.675	35.1	333	0.440	9.853	308	0.705	25.4	370	0.500	7.529
126	0.675	35.1	333	0.513	9.773	309	0.705	25.4	370	0.546	7.629
127	0.675	35.1	333	0.586	9.702	310	0.705	25.4	370	0.593	7.626
128	0.675	35.1	333	0.659	9.621	311	0.705	25.4	370	0.640	7.654
129	0.675	35.1	333	0.732	9.540	312	0.705	25.4	370	0.687	7.590
130	0.675	35.1	333	0.771	8.310	313	0.705	25.4	370	0.711	7.675
131	0.675	35.1	321	0.006	10.479	314	0.712	50.0	463	0.051	15.184
132	0.675	35.1	321	0.082	10.323	315	0.712	50.0	463	0.126	14.377
133	0.675	35.1	321	0.158	10.134	316	0.712	50.0	463	0.202	13.584
134	0.675	35.1	321	0.233	10.065	317	0.712	50.0	463	0.277	13.134
135	0.675	35.1	321	0.309	9.986	318	0.712	50.0	463	0.352	12.876
136	0.675	35.1	321	0.385	9.886	319	0.712	50.0	463	0.428	12.724
137	0.675	35.1	321	0.461	9.807	320	0.712	50.0	463	0.503	12.520
138	0.675	35.1	321	0.537	9.718	321	0.712	50.0	463	0.578	12.369
139	0.675	35.1	321	0.613	9.638	322	0.712	50.0	463	0.654	12.239
140	0.675	35.1	321	0.689	9.549	323	0.712	50.0	463	0.729	12.079
141	0.675	35.1	321	0.765	8.820	324	0.712	50.0	463	0.769	10.234
142	0.675	35.1	321	0.805	7.330	325	0.714	50.0	836	0.012	15.317
143	0.675	30.0	676	0.031	8.340	326	0.714	50.0	836	0.053	14.930
144	0.675	30.0	676	0.069	8.270	327	0.714	50.0	836	0.095	14.652
145	0.675	30.0	676	0.100	8.210	328	0.714	50.0	836	0.137	14.163
146	0.675	30.0	676	0.130	8.230	329	0.714	50.0	836	0.179	13.784
147	0.675	30.0	676	0.161	8.260	330	0.714	50.0	836	0.221	13.092

Table 1. Continued

no.	p / MPa	q / kW·m^{-2}	G / kg·m^{-2}·s^{-1}	x	h / kW·m^{-2}·K^{-1}	no.	p / MPa	q / kW·m^{-2}	G / kg·m^{-2}·s^{-1}	x	h / kW·m^{-2}·K^{-1}
148	0.675	30.0	676	0.191	8.190	331	0.714	50.0	836	0.263	12.823
149	0.675	30.0	676	0.222	8.290	332	0.714	50.0	836	0.304	12.680
150	0.675	30.0	676	0.252	8.280	333	0.714	50.0	836	0.346	12.558
151	0.675	30.0	676	0.283	8.270	334	0.714	50.0	836	0.368	12.475
152	0.675	30.0	676	0.313	8.290	335	0.720	30.0	400	0.001	8.857
153	0.675	30.0	676	0.344	8.210	336	0.720	30.0	400	0.066	8.784
154	0.675	30.0	676	0.375	8.280	337	0.720	30.0	400	0.131	8.754
155	0.675	30.0	676	0.405	8.270	338	0.720	30.0	400	0.196	8.756
156	0.675	30.0	676	0.421	8.280	339	0.720	30.0	400	0.248	8.677
157	0.675	30.0	518	0.038	8.330	340	0.720	30.0	400	0.299	8.714
158	0.675	30.0	518	0.088	8.220	341	0.720	30.0	400	0.351	8.666
159	0.675	30.0	518	0.139	8.290	342	0.720	30.0	400	0.403	8.661
160	0.675	30.0	518	0.179	8.200	343	0.720	30.0	400	0.455	8.583
161	0.675	30.0	518	0.219	8.210	344	0.720	30.0	400	0.507	8.619
162	0.675	30.0	518	0.259	8.270	345	0.720	30.0	400	0.559	8.530
163	0.675	30.0	518	0.299	8.230	346	0.720	30.0	400	0.610	8.587
164	0.675	30.0	518	0.340	8.260	347	0.720	30.0	400	0.662	8.602
165	0.675	30.0	518	0.380	8.290	348	0.720	30.0	400	0.714	8.566
166	0.675	30.0	518	0.420	8.310	349	0.720	30.0	400	0.766	7.588
167	0.675	30.0	518	0.460	8.190	350	0.720	30.0	400	0.793	6.414
168	0.675	30.0	518	0.500	8.240	351	0.727	25.4	370	0.050	7.853
169	0.675	30.0	518	0.541	8.260	352	0.727	25.4	370	0.109	7.794
170	0.675	30.0	518	0.581	8.210	353	0.727	25.4	370	0.169	7.555
171	0.675	30.0	518	0.602	8.250	354	0.727	25.4	370	0.216	7.574
172	0.675	30.0	400	0.021	8.578	355	0.727	25.4	370	0.264	7.624
173	0.675	30.0	400	0.086	8.508	356	0.727	25.4	370	0.311	7.653
174	0.675	30.0	400	0.151	8.480	357	0.727	25.4	370	0.359	7.650
175	0.675	30.0	400	0.216	8.481	358	0.727	25.4	370	0.406	7.721
176	0.675	30.0	400	0.268	8.405	359	0.727	25.4	370	0.454	7.739
177	0.675	30.0	400	0.320	8.440	360	0.727	25.4	370	0.501	7.652
178	0.675	30.0	400	0.372	8.394	361	0.727	25.4	370	0.549	7.753
179	0.675	30.0	400	0.424	8.389	362	0.727	25.4	370	0.596	7.750
180	0.675	30.0	400	0.477	8.312	363	0.727	25.4	370	0.644	7.778
181	0.675	30.0	400	0.529	8.347	364	0.727	25.4	370	0.691	7.712
182	0.675	30.0	400	0.581	8.261	365	0.727	25.4	370	0.716	7.798
183	0.675	30.0	400	0.633	8.316						

4. Results and Discussion

Local flow boiling heat transfer coefficients are investigated over a range of vapor qualities up to 0.8. The mass flux varies from (310 to 860) kg·m^{-2}·s^{-1}. The heat flux ranges from (21 to 50) kW·m^{-2}, and the saturation pressure changes from (0.65 to 0.75) MPa. The heat transfer coefficient measured falls in the range of (6 to 15.5) kW·m^{-2}·K^{-1}. The measured data are given in Table 1.

Figures 3, 4, 5, and 6 show the dependences of the heat transfer coefficient on vapor quality under different saturation pressures (average pressures of the inlet and the outlet) and heat fluxes. The heat transfer coefficients decrease with increasing vapor quality except those in the low heat and mass flux conditions. Because there is always a large pressure drop in mini-channel flow boiling experiments, especially in the high heat and mass flux conditions, it is unclear that how severe the pressure drop contributes to the heat transfer coefficient decrease. For this reason, we correlate more than 500 experimental data in this study, and the results show a moderate dependence of heat transfer coefficient on saturation pressure, namely, $h \propto p^{0.43}$. Although we are not able to confirm if this

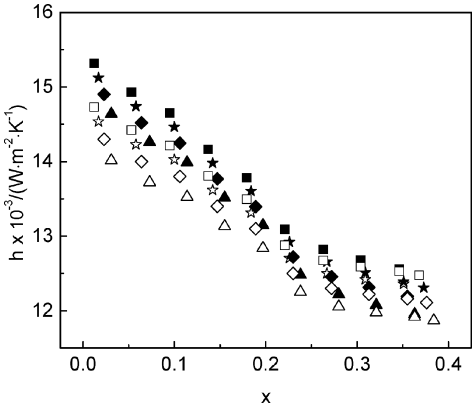

Figure 3. Dependences of the heat transfer coefficient h on vapor quality x under different saturation pressures at $q = 50.0$ kW·m^{-2} and $G = 836$ kg·m^{-2}·s^{-1}. Both the original and the recalculated heat transfer coefficients are drawn. The solid symbols represent the original data, and the open symbols represent the corrected data. ▲ and △, $p = 0.651$ MPa; ◆ and ◇, $p = 0.675$ MPa; ★ and ☆, $p = 0.696$ MPa; ■ and □, $p = 0.714$ MPa.

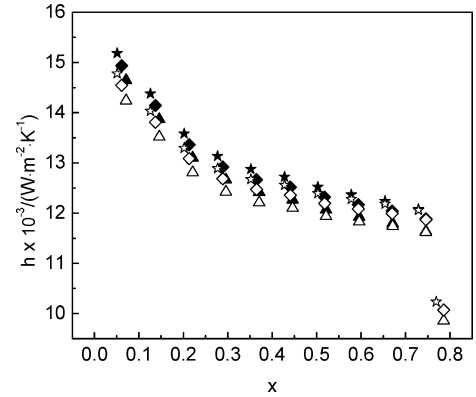

Figure 4. Dependences of the heat transfer coefficient h on vapor quality x under different saturation pressures at $q = 50.0$ kW·m^{-2} and $G = 463$ kg·m^{-2}·s^{-1}. The solid symbols represent the original data, and the open symbols represent the corrected data. ▲ and △, $p = 0.675$ MPa; ◆ and ◇, $p = 0.694$ MPa; ★ and ☆, $p = 0.712$ MPa.

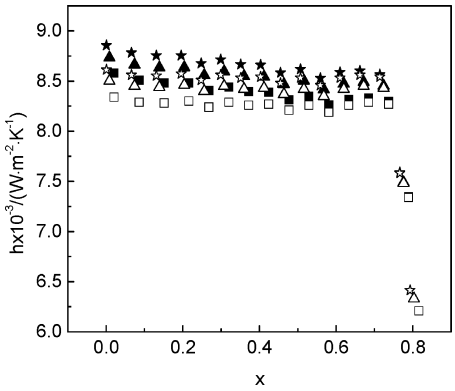

Figure 5. Dependences of the heat transfer coefficient h on vapor quality x under different saturation pressures at $q = 30.0$ kW·m^{-2} and $G = 400$ kg·m^{-2}·s^{-1}. The solid symbols represent the original data, and the open symbols represent the corrected data. ▲ and △, $p = 0.675$ MPa; ◆ and ◇, $p = 0.701$ MPa; ★ and ☆, $p = 0.720$ MPa.

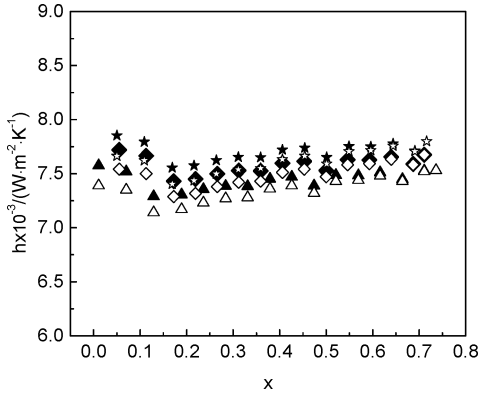

Figure 6. Dependences of the heat transfer coefficient h on vapor quality x under different saturation pressures at $q = 25.4$ kW·m^{-2} and $G = 370$ kg·m^{-2}·s^{-1}. Both the original and the recalculated heat transfer coefficients are drawn. The solid symbols represent the original data, and the open symbols represent the corrected data. ▲ and △, $p = 0.675$ MPa; ◆ and ◇, $p = 0.705$ MPa; ★ and ☆, $p = 0.727$ MPa.

dependence comes from a boiling suppression because of the high pressure in this study, we try to eliminate or at least weaken the effect of the large pressure drop by dividing the measured local heat transfer coefficients by a factor of $(p/p_o)^{0.43}$, where p_o is the pressure at the outlet of each experimental run. Both the original and the recalculated heat transfer coefficients are drawn in Figures 3, 4, 5, and 6 where the solid symbols represent the original data and the open symbols represent the corrected data. Though the effect of the large pressure drop cannot be completely eliminated by this method, it can be concluded that the pressure drop is obviously not the only factor which contributes to the decrease of the heat transfer coefficient with increasing vapor quality.

The dependences of the heat transfer coefficient on vapor quality under different heat and mass fluxes are depicted in Figures 7, 8, 9, and 10. As are shown in the figures, the dependences of the heat transfer coefficient on mass flux vary with different heat fluxes. In high heat flux conditions, the heat transfer coefficients are almost independent of mass flux. While at a lower heat flux of 25.4 kW·m^{-2}, the heat transfer coefficient shows observable dependence on mass flux. Similarly, the dependences of the heat transfer coefficient on vapor quality also vary with different heat fluxes. In high heat flux conditions, the heat transfer coefficient decreases quickly with increasing vapor quality, as shown in Figures 7 and 8. When the heat flux decreases, this decreasing trend gets weaker. The heat transfer

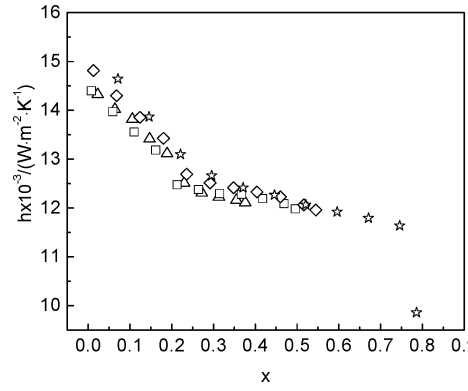

Figure 7. Dependence of the heat transfer coefficient h on vapor quality x under different mass fluxes at $q = 50.0$ kW·m^{-2} and an average saturation pressure of 0.675 MPa. △, $G = 836$ kg·m^{-2}·s^{-1}; □, $G = 676$ kg·m^{-2}·s^{-1}; ◇, $G = 621$ kg·m^{-2}·s^{-1}; ☆, $G = 463$ kg·m^{-2}·s^{-1}.

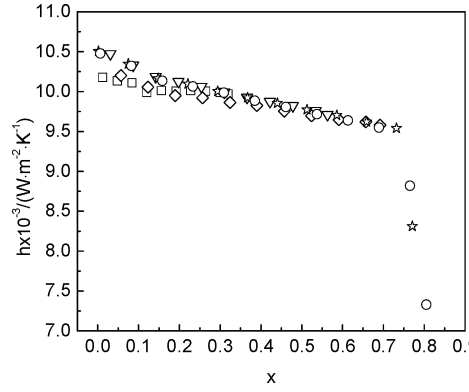

Figure 8. Dependence of the heat transfer coefficient h on vapor quality x under different mass fluxes at $q = 35.1$ kW·m^{-2} and an average saturation pressure of 0.675 MPa. □, $G = 676$ kg·m^{-2}·s^{-1}; ▽, $G = 436$ kg·m^{-2}·s^{-1}; ◇, $G = 365$ kg·m^{-2}·s^{-1}; ☆, $G = 333$ kg·m^{-2}·s^{-1}; ○, $G = 321$ kg·m^{-2}·s^{-1}.

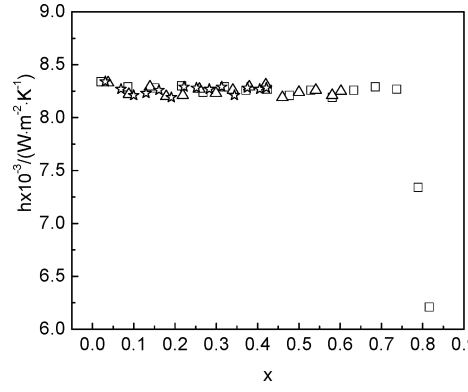

Figure 9. Dependence of the heat transfer coefficient h on vapor quality x under different mass fluxes at $q = 30.0$ kW·m^{-2} and an average saturation pressure of 0.675 MPa. □, $G = 676$ kg·m^{-2}·s^{-1}; △, $G = 518$ kg·m^{-2}·s^{-1}; ☆, $G = 400$ kg·m^{-2}·s^{-1}.

coefficient even increases with vapor quality when the heat flux is reduced to a low heat flux of 25.4 kW·m^{-2}. It appears in the figures that the heat flux of 30.0 kW·m^{-2} is a turning point in the current experiment. Near the turning point, the heat transfer coefficient is insensitive to the vapor quality. In addition, for many experimental runs, the heat transfer coefficient decreases sharply at a vapor quality of about 0.75.

Figure 11 plots the dependence of the heat transfer coefficient on vapor quality under different heat fluxes but the same mass flux. As shown in the figure, the heat transfer coefficient always

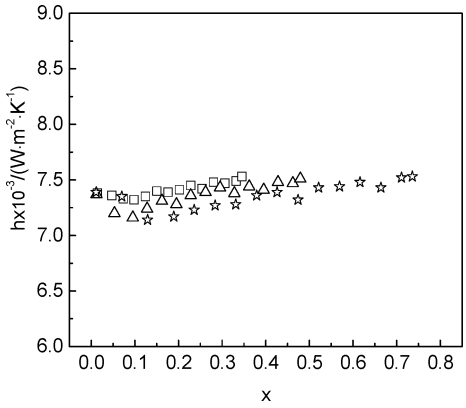

Figure 10. Dependence of the heat transfer coefficient h on vapor quality x under different mass fluxes at $q = 25.4$ kW·m^{-2} and an average saturation pressure of 0.675 MPa. □, $G = 676$ kg·m^{-2}·s^{-1}; △, $G = 527$ kg·m^{-2}·s^{-1}; ☆, $G = 370$ kg·m^{-2}·s^{-1}.

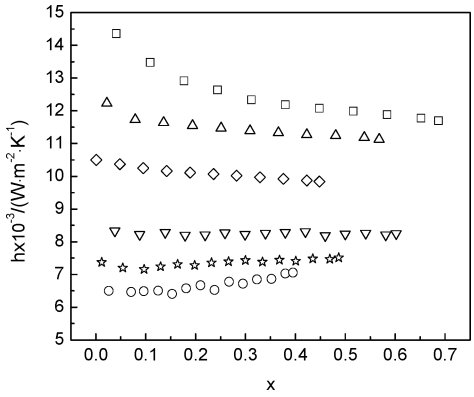

Figure 11. Dependence of the heat transfer coefficient h on vapor quality x under different heat fluxes at $G = 518$ kg·m^{-2}·s^{-1}. □, $q = 50.0$ kW·m^{-2}; △, $q = 42.9$ kW·m^{-2}; ◇, $q = 35.1$ kW·m^{-2}; ▽, $q = 30.0$ kW·m^{-2}; ☆, $q = 25.4$ kW·m^{-2}; ○, $q = 21.1$ kW·m^{-2}.

increases with increasing heat flux, which is identified with the nucleate boiling dominant heat transfer mechanism.

It is often accepted that saturated flow boiling heat transfer is governed by two mechanisms: nucleate boiling and convective boiling. For saturated flow boiling heat transfer in a mini channel, nucleate boiling and convective boiling are also thought to be the governing mechanisms.[15] Therefore, the methods based on these two mechanisms are frequently applied to analyze the mini-channel experiments. Some experiments[3,5,16,18] demonstrated that the flow boiling heat transfer coefficient strongly depended on heat flux and saturation pressure while hardly on mass flux and vapor quality, up to vapor qualities high as (60 to 70) %. The authors claimed that nucleate boiling dominates the heat transfer. In contrast, some other experiments[17,19] showed that the heat transfer coefficient increased with the increasing vapor quality and mass flux except in a small region with low vapor qualities of (0 to 20) %. The results were explained in the forced convective dominated boiling regime. Still, some researchers[9,10] found that the heat transfer coefficient started to decrease with increasing vapor quality at the very beginning of a saturated boiling when the heat flux reached a certain level. It appears that the conventional method, with only nucleate boiling and convective boiling contributions, is insufficient to explain the mini-channel flow boiling experiments. This difficulty will be partially solved if the helpful conception of periodic dry-out is introduced. This conception was proposed by Thome at al.[20] In Thome's model, bubbles are assumed to nucleate and quickly grow to the channel's size such that

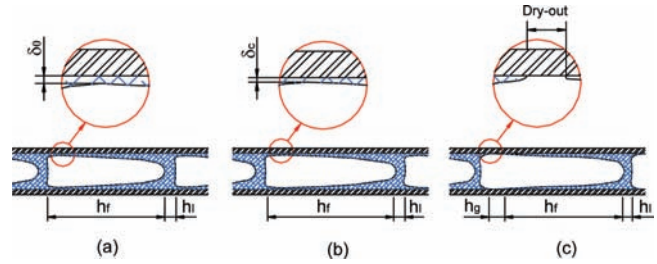

Figure 12. Schematic drawing of the three-zone heat transfer model.

successive elongated bubbles are formed, confined radially by the tube wall, and grow in length, trapping a thin film of liquid between the bubble and the inner tube wall. Then, dry-out promptly occurs at the tail of the liquid film at the onset of saturated boiling. On the basis of this concept, a three-zone heat transfer model, which includes liquid film, liquid slug, and dry-out region are established and schematically shown in Figure 12. For explanation convenience, the time-average heat transfer coefficients of dry-out, liquid film, and liquid slug regions are defined as h_g, h_f, and h_l, respectively.

In the current experiment, with a horizontal stainless steel mini tube of 1.3 mm inner diameter, dry-out may appear at the very onset of saturation boiling when the heat flux is higher than 30.0 kW·m^{-2}. When the vapor quality increases, the period of dry-out becomes longer, and the proportion of h_g increases. Meanwhile, the weights of h_f and h_l decrease, which explains the decreasing trend of heat transfer coefficient with vapor quality as shown in Figures 7, 8, and 11. In addition, since h_f denotes the thin liquid film evaporation heat transfer coefficient and is the main contributor of the heat transfer coefficient in this region, the contribution of h_l to the whole heat transfer is comparatively small. Consequently, the heat transfer coefficient shows almost independence upon mass flux.

When the heat flux is around 30 kW·m^{-2}, traditional bubbly flow is probably suited for the region of low vapor quality. In the region of high vapor quality, the three-zone model is appropriate, but the h_f may not be as high as in the high heat flux region, so the increase of h_g or h_l may balance the decrease resulting from the increasing period of dry-out. Therefore, the heat transfer coefficient is less sensitive to the vapor quality as is shown in Figures 9 and 11.

When the heat flux is less than 30.0 kW·m^{-2}, dry-out may not exist at all. The three-zone heat transfer model should be degraded to a two-zone model, which only includes liquid film and liquid slug, as shown in Figure 12a,b. As a consequence, the convective evaporation is the main contributor of the flow boiling heat transfer, and the heat transfer coefficient increases with increasing mass flux and vapor quality.

In addition, a sharp decrease of the heat transfer coefficient is also observed at a vapor quality of about 0.75. This point is likely the flow pattern transition from annular flow to annular-mist flow.

5. Conclusions

According to the experimental results and analysis, the following conclusions can be drawn:

1. The heat transfer coefficient always increases with the increase of saturation pressure and heat flux.

2. A turning value of the heat flux, approximately 30.0 kW·m^{-2}, is observed in our experiments. When the heat flux is lower than this turning value, the heat transfer coefficient increases with increasing mass flux and vapor quality. When the heat flux is larger than the turning value, the heat transfer

coefficient decreases with increasing vapor quality but is insensitive to the mass flux. Near the turning heat flux, the heat transfer coefficient is insensitive to both the mass flux and the vapor quality.

3. Dry-out is an important concept in mini-channel flow boiling. The heat transfer behavior depends on the competition between the decrease of the heat transfer coefficient resulting from the increase of dry-out and the increase of the heat transfer coefficient contributed by the thin liquid film evaporation.

Literature Cited

(1) Wadekar, V. V. Flow boiling of heptane in a plate-fin heat exchangers passage, Compact Heat Exchangers for Power and Process Industries, HTD. *Proc. ASME Heat Transfer Div.* **1993**, *201*, 1–6.

(2) Carey, V. P. Two-phase flow in small-scale ribbed and finned passages for compact evaporators and condensers. *Nucl. Eng. Des.* **1993**, *141*, 249–268.

(3) Kew, P. A.; Cornwell, K. Correlations for the prediction of boiling heat transfer in small-diameter channels. *Appl. Therm. Eng.* **1997**, *17*, 705–715.

(4) Wilmarth, T.; Ishii, M. Two-phase flow regimes in narrow rectangular vertical and horizontal channels. *Int. J. Heat Mass Transfer* **1994**, *37*, 1749–1758.

(5) Wambsganss, M. W.; France, D. M.; Jendrzejczyk, J. A.; Tran, T. N. Boiling heat transfer in a small-diameter tube. *J. Heat Transfer* **1993**, *115*, 963–972.

(6) Oh, H.; Katsuta, M.; Shibata, K. Heat transfer characteristics of R134a in a capillary tube heat exchanger. *Proc. Int. Heat Transfer Conf. 11th* **1998**, *6*, 131–136.

(7) Zhang, W.; Hibiki, T.; Mishima, K. Correlation for flow boiling heat transfer at low liquid Reynolds number in small diameter channels. *J. Heat Transfer* **2005**, *127*, 1214–1221.

(8) Bertsch, S. S.; Groll, E. A.; Garimella, S. V. Effect of heat flux, mass flux, and saturation temperature on flow boiling heat transfer in microchannels. *Int. J. Multiphase Flow* **2009**, *35*, 142–154.

(9) Lin, S.; Kew, P. A.; Cornwell, K. Two-phase heat transfer to a refrigerant in a 1 mm diameter tube. *Int. J. Refrig.* **2001**, *24*, 51–56.

(10) Huo, X.; Chen, L.; Tian, Y. S.; Karayiannis, T. G. Flow boiling and flow regimes in small diameter tubes. *Appl. Therm. Eng.* **2004**, *24*, 1225–1239.

(11) Shiferaw, D.; Karayiannis, T. G.; Kenning, D. B. R. Flow boiling in a 1.1 mm tube with R134a: Experimental results and comparison with model. *Int. J. Therm. Sci.* **2009**, *48*, 331–341.

(12) *ASHRAE Handbook Fundamentals 2005*; American Society of Heating, Refrigerating, and Air-Conditioning Engineers: Atlanta, GA, 2005.

(13) Tran, T. N.; Wambsganss, M. W.; France, D. M. Small circular and rectangular channel boiling with two refrigerants. *Int. J. Multiphase Flow* **1996**, *22*, 485–498.

(14) Moffat, R. J. Describing the uncertainties in the experimental results. *Exp. Therm. Fluid Sci.* **1988**, *1*, 3–17.

(15) Kandlikar, S. G. Heat Transfer Mechanisms During Flow Boiling in Microchannels. *J. Heat Transfer* **2004**, *126*, 8–16.

(16) Bao, Z. Y.; Fletcher, D. F.; Haynes, B. S. Flow boiling heat transfer of R11 and R123 in narrow passages. *Int. J. Heat Mass Transfer* **2001**, *43*, 3347–3358.

(17) Lazarek, G. M.; Black, S. H. Evaporative heat transfer, pressure drop and critical heat flux in a small diameter vertical tube with R113. *Int. J. Heat Mass Transfer* **1982**, *25*, 945–960.

(18) Vlasie, C.; Macchi, H.; Guilpart, J.; Agostini, B. Flow boiling in small channels. *Int. J. Refrig.* **2004**, *27*, 191–201.

(19) Kureta, M.; Kobayashi, T.; Mishima, K.; Nshihara, H. Pressure drop and heat transfer for flow boiling of water in small-diameter tubes. *JSME Int. J., Ser. B* **1998**, *41*, 871–879.

(20) Thome, J. R.; Dupont, V.; Jacobi, A. M. Heat transfer model for evaporation in microchannels. *Int. J. Heat Mass Transfer* **2004**, *47*, 3375–3385.

Received for review January 30, 2009. Accepted July 6, 2009. We thank the Scientific Research Foundation for the Returned Overseas Chinese Scholars by the Ministry of Education in China and the Alexander von Humboldt Foundation in Germany for financial support.

JE900140W